Catalytic CO_2 Reduction Using an Atomically Precise, Cu-Coordinated, Crystalline Carbon Nitride

Magnus Pauly,[1] Mawuli Deegbey,[1] Landon Keller,[2] Scott McGuigan,[1] Golnaz Dianat,[2] Jian Cheng Wong,[3,4] Corban G.F. Murphey,[3] Bo Shang,[5] Hailiang Wang,[5] James F. Cahoon,[3] Renato Sampaio,[3] Yosuke Kanai,[3,4] Gregory Parsons,[2] Elena Jakubikova,[1] and Paul A. Maggard[1,*]

[1] North Carolina State University, Department of Chemistry, Raleigh, NC 27695; [2] North Carolina State University, Department of Chemical Engineering, Raleigh, NC 27695; [3] University of North Carolina-Chapel Hill, Department of Chemistry, Chapel Hill, NC 27599; [4] University of North Carolina-Chapel Hill, Departments of Physics and Astronomy, Chapel Hill, NC 27599; [5] Yale University, Department of Chemistry, New Haven, CT 06520

KEYWORDS. Electrocatalytic CO_2 reduction, crystalline carbon nitride, electrophoretic deposition, electronic structure calculations, mechanistic pathway

ABSTRACT: Inherently disordered structures of carbon nitrides have hindered an atomic level tunability and understanding of their catalytic reactivity. Herein, coordination of copper cations within a crystalline carbon nitride, i.e., poly(triazine imide) or CN_x, was found to yield two ordered structures for Cu-CN_x wherein one or two Cu(I) cations coordinate to its intralayer N-triazine groups. The crystallites electrophoretically deposit from aqueous particle suspensions and yield current densities of ~10 to 50 mA/cm^2 with a concomitant and increasing reduction of CO_2 and H_2O. Reduction of CO_2 increases for smaller particles as mechanistic calculations reveal its catalysis mediated by two intralayer Cu atoms.

At this present moment the production of carbon dioxide (CO_2) from fossil fuels is a global issue, with our daily life tied to processes which release billions of metric tons of CO_2 per year. To address this, intense research has gone into the capture and conversion of CO_2 into fuels. Research into carbon nitrides has surged in importance because of their promising catalytic activities for the reduction of carbon dioxide (CO_2R), such as when impregnated with metals, and producing carbon monoxide, formate, and/or methanol.[1–6] While promising, these materials lack sufficient crystallinity for in depth structural characterization of the local coordination environments or determination of mechanistic pathways with atomic-level detail. Relevant mechanisms are hypothesized assuming idealized models.

Most studied carbon nitrides are layered but amorphous materials containing heptazine monomers with alternating sp^2 carbon and nitrogen. The carbon to nitrogen ratio is typically C_3N_4, or otherwise known as graphic carbon nitride (g-C_3N_4).[7] A more highly crystalline carbon nitride, poly(triazine imide)·Li_2Cl (PTI/LiCl; $C_6N_9H_2Li_2Cl$), consists of triazine rings linked by imide bridges. Notably, it also contains intralayer cavities with two Li and two H cations each.[8,9] A recent study of the different possible Li/H configurations demonstrated a preferred cation ordering within its intralayer cavities.[10] The crystalline PTI/LiCl was also shown to possess the capability to coordinate a small amount of transition-metal cations (e.g., Cu(I)) with the maintenance of its structure.

The extent and impact of Cu coordination within the crystalline PTI/LiCl structure, as well as for its activity for CO_2R, has been found to yield highly ordered structures for understanding product formation and mechanistic pathways at the atomic level. Crystalline PTI/LiCl was prepared according to prior literature[10] and reacted with either a eutectic mixture of CuCl/KCl (60:40) or $CuCl_2$/KCl (55:45), yielding PTI/Cu-low and PTI/Cu-high, respectively. Details are provided in the Supporting Information. Both attained a maximal amount of Cu cations, on average, of one per cavity. However, powder XRD data showed significant differences, with refinements yielding different configurations and contents for their cavities.

The structures of both PTI/Cu-low and -high both generally show the maintenance of the underlying carbon nitride framework upon coordination by the Cu cations, visualized in Figure

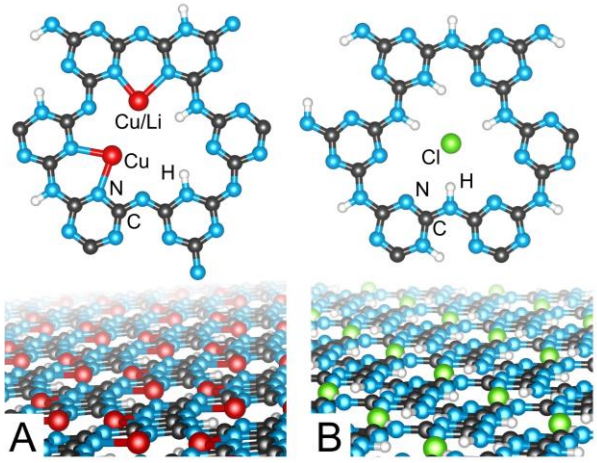

Figure 1. Extended structural views of single layers (lower) and isolated intralayer cavities (upper) of the (A) Cu-containing layer for PTI/Cu-low (1 Cu, 1 Li) and PTI/Cu-high (2 Cu, 0 Li) and the (B) additional delithiated layer only present in the structure of PTI/Cu-high.

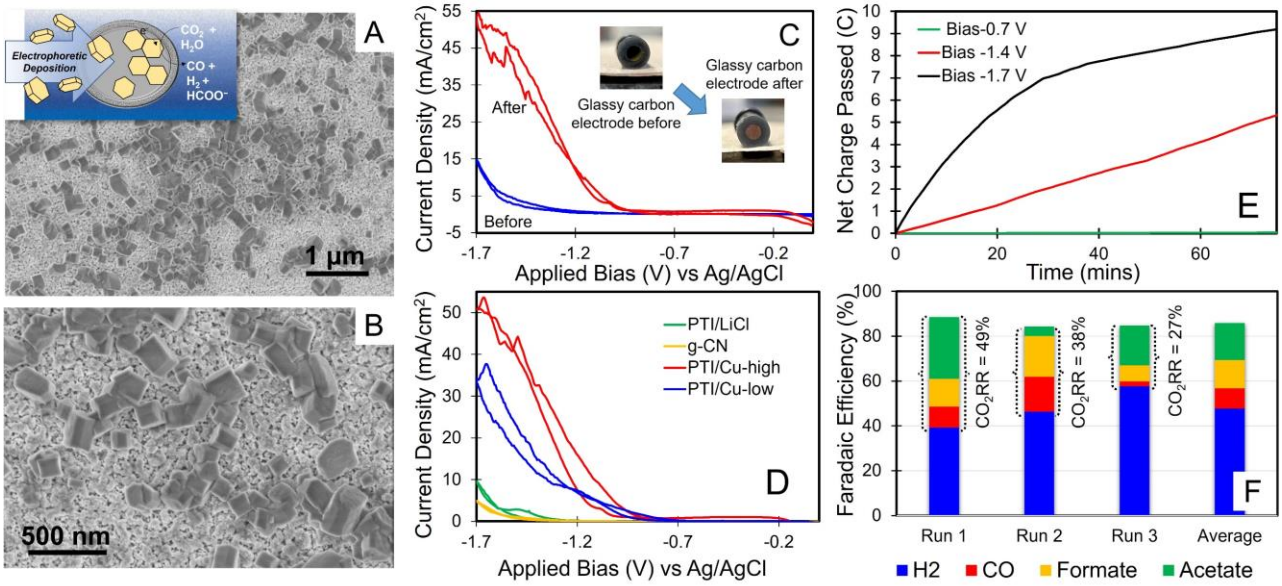

Figure 2. (A,B) SEM image of PTI/Cu-high particles deposited onto an FTO electrode after 90 min, (C) cyclic voltammetry (CV) of PTI/Cu-high, both before and after photoelectrophoretic deposition for 22 h in 0.5M $KHCO_3$, (D) CV's of PTI/Cu-high, -low and control samples of PTI/LiCl and g-CN, (E) charged passed with time at different applied biases for PTI/Cu-high, and (F) Faradaic efficiencies

1. Rietveld refinement of the carbon nitride structure of PTI/Cu-low shows it maintains the parent PTI/LiCl structure with one Li cation replaced by Cu per cavity, on average. However, significant differences occur for the structure of PTI/Cu-high. Rietveld refinements of PTI/Cu-high could not be matched with any of the reported, 20 possible ordered or partially-disordered polymorphs.[9,10] Attempted structural solutions instead revealed a mixture of two types of layers, Figure 1 (A and B), that stack together. One consists of a de-lithiated layer wherein the chloride anion is located within the cavity with four N-H protons, Figure 1A, as reported for the structure of PTI·HCl.[11,12] The other layer contains two Cu cations per cavity at ~3.9Å apart, Figure 1B, in a tetrahedral coordination environment with Cu-Cl (×2; not shown in Figure 1 for clarity) and Cu-N (×2). A 50:50 ratio of the two layers also yields an average of ~1 Cu atom per cavity. The PTI/Cu-low and PTI/Cu-high compositions and structures are consistent with elemental analysis from ICP-OES ($C_6N_9H_{2.3}CuCl$ and $C_6N_9H_{4.1}CuCl$) as well as FT-IR (Supporting Information) that shows a growth in the H content and N-H stretching region for the latter.

Catalytic CO_2R has been intensely investigated for Cu-containing, N-doped graphene and for many of its molecular complexes.[1-6,13] The former is disordered and the latter complexes decompose at the electrode surface, so atomically-precise catalytic pathways remain unclear.[14] To shed new light onto the reasons for this difficulty, films of the PTI/Cu materials were achieved using a new low-bias, electrophoretic deposition of the particles from an aqueous 0.5M $KHCO_3$. While this technique has typically required 100's of volts, particles of PTI/Cu could be deposited at only -1.4V versus Ag/AgCl in an H-cell cathodic compartment, Figure 2 (A and B) after 90 min. Well-formed crystallites of increasing size are found to deposit, ranging from very fine (initially) to much larger ~250 nm crystallites later. The crystallites were deposited onto either FTO or glassy carbon over the course of up to 22 h and, after deposition, yielded a cathodic current density of ~1 to 5 mA cm^{-2} at -1.4 V and the electrocatalytic reduction of protons and CO_2. The cyclic voltammograms (CV), pre- versus post-deposition, yield a significantly enhanced current density of ~30 to 50 mA cm^{-2} at -1.7V, Figure 2C. Neither PTI/LiCl nor g-CN showed a similar response, Figure 2D, confirming the deposition and CO_2R catalytic activity arises from the Cu-containing PTI/Cu.

At an applied bias of -1.4 V versus Ag/AgCl, Figure 2E, stable films were obtained that gave Faradaic efficiencies (FE), for acetate (~10-20%), formate (~10-20%), H_2 (~50%), and CO (~9%). While the FE varied from run to run, a larger amount of CO_2R was found to occur with the smallest crystallites deposited from the initial aqueous suspension, Figure 2F. In electrophoretic deposition it is established that the smallest crystallites will deposit the fastest,[15,16] with sequential depositions resulting in increasingly larger crystallites on the substrate, giving FE for

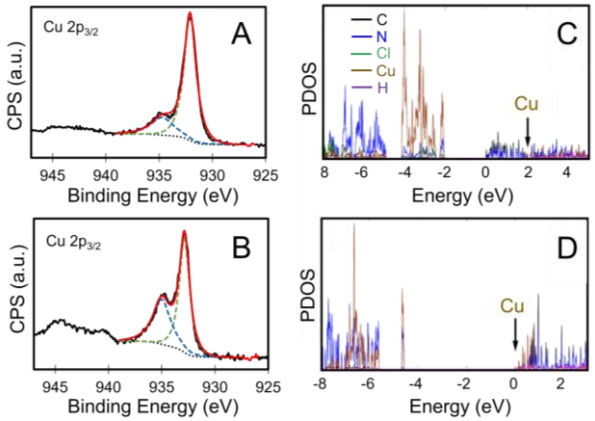

Figure 3. *Ex-situ* XPS high resolution spectra Cu $2p_{3/2}$ region for PTI/Cu-high before reaction (A) and after reaction on the electrode (B), including experimental (black-solid), background (black-dotted), fitted Cu(0)/Cu(I) peak (green-dashed), fitted Cu (II) peak (blue-dashed), and total fitted signal (red-solid). Projected density of states (PDOS) on atomic orbitals, based on the quasi-particles energies obtained at G_0W_0@PBE0 level of theory for (C) bulk PTI/Cu and (D) monolayer PTI/Cu. Conduction band minimum (CBM) is set as the reference energy (i.e., E = 0 eV).

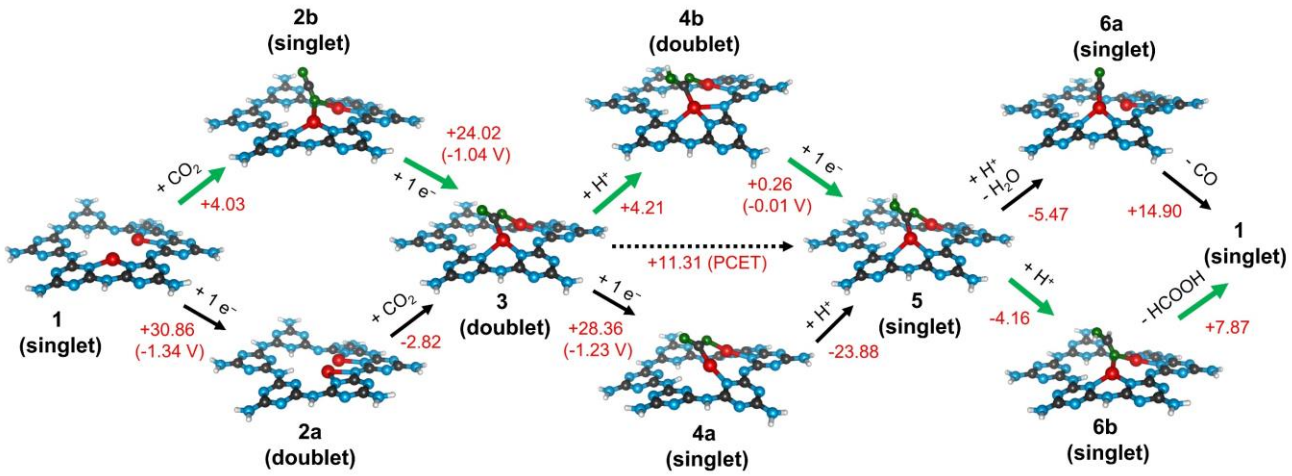

Figure 4. Electrocatalytic CO_2R reduction of CO_2 to CO and HCOOH on PTI/Cu-high, with green arrows labeling the lowest energy pathway. Thermodynamic data reported in kcal/mol and redox potential in V vs Ag/AgCl (in parentheses).

CO_2R that decreases from 49% to 38% and then to 27%. The range of crystallite sizes depositing from solution also likely leads to some particle distribution inhomogeneities and to the FE varying within ±10% between CO_2R experiments.

While electron microscopy confirmed the crystallite morphologies and elemental compositions remained stable and unchanged during the CO_2R experiments, XPS measurements were used to track possible changes in the Cu oxidation states and coordination environments closer to the surfaces. XPS data confirm that the relative at. % of N, Cu, Cl and Li remain consistent both before and after CO_2R experiments, see Supporting Information. After CO_2R, the *ex-situ* XPS data in Figure 3 (A, B) show the Cu(I) feature remains dominant to the Cu(II) feature, and the Auger Cu $L_3M_{45}M_{45}$ parameter (Supporting Information) is consistent with CuCl and $CuCl_2$ bonding environment before and after CO_2R, in agreement with the coordination environment of the Cu cation in PTI/Cu-high.[17] These data confirm that both the crystallites and their Cu-coordination sites within the intralayer cavities at the surfaces of the carbon nitride are either maintained, or reversibly recovered, before and after the CO_2R experiments.

First-principles electronic structure theory was employed to analyze both the bulk and two-dimensional (2D) monolayer form of PTI/Cu for insights into how the substitution of Li for Cu cations impacts the electronic structure of PTI and the ability to facilitate CO_2R at its band edges.[18] Specifically, the GW method was utilized in the framework of many-body Green's function theory, starting with PBE0 hybrid exchange-correlation density functional theory (DFT) calculation.[19-21] Figure 3 (C, D) shows the atom-projected density of states (DOS) of the bulk and monolayer form of PTI/Cu. The main difference in the DOS is observed in the band gap and conduction band (CB) energy. As the bulk PTI becomes more of two-dimensional (2D) and reaches a monolayer limit, the band gap increases and Cu-based states increasingly shift to dominate at the bottom of the CB edge. While the PTI/Cu crystallites have different sizes and thicknesses, these results indicate that the highest activities for CO_2R is associated with the concomitant shifting of the Cu states closer to the CB edge with decreasing particle thickness. The maximal rates should thus be obtainable at the monolayer limits, consistent with the CO_2R experiments.

Next, density-functional theory calculations were employed to elucidate the thermodynamics of the electrocatalytic reduction of CO_2 to CO and formate. Shown in Figure 4 is the resulting mechanistic scheme with the calculated binding energies and reduction potentials. The first and second reduction potentials of the starting complex were calculated. However, due to the instability of the doubly reduced complex, only the calculated first reduction potential of -1.34 V vs Ag/AgCl is shown. To begin the catalytic cycle, adsorption of CO_2 on the two Cu sites of the complex ($[PTI\text{-}Cu_2]^+$) may occur either before or after the one-electron reduction. The free energy of CO_2 binding after the first reduction (-2.82 kcal/mol) is more favorable than the initial binding of CO_2 to the two Cu sites of the starting complex (+4.03 kcal/mol). This occurs because of shifting of the two Cu atoms closer together after reduction. The reduction potential after CO_2 binding is -1.04 V vs Ag/AgCl. Based on the reasonable agreement between the first reduction potential at the applied bias potential of about -1.0 V vs Ag/AgCl in Figure 2, as well as the calculated exergonic CO_2 binding energy after the first reduction, this indicates that CO_2 binds to the two Cu atoms after their reduction which begins the catalytic cycle.

The coordinated CO_2 complex (3; $[PTI\text{-}Cu_2\text{-}CO_2]$) can undergo a reduction reaction followed by protonation or protonation followed by reduction to form the intermediate, [5; PTI-Cu-COOH]. Next, subsequent protonation of the intermediate on the terminal hydroxyl group and the release of H_2O steers the cycle towards CO formation, while protonation of the carbon leads to formate. For the CO cycle, protonation with the release of H_2O is thermodynamically favorable, with a free energy of -5.47 kcal/mol. Desorption of CO is an uphill process (ΔG = + 14.89 kcal/mol), indicating that its release is less favorable. An uphill process is also observed for the desorption of formic acid (ΔG = + 7.87 kcal/mol), at a relatively smaller free energy. The two-fold decrease in the free energy with the release of formate suggests its greater selectivity as compared to CO, as observed experimentally. The formation of CO as an intermediate is also consistent with pathways leading to acetate formation. However, C-C coupling leading to acetate could proceed via multiple different pathways (>10 known possibilities),[22] and thus this more complex mechanistic pathway is under ongoing investigation.

Particularly notable is the shifting of the Cu cation out of the plane of the intralayer cavity, especially after the second electron reduction as a result of the change in local coordination environment preferences of Cu(I)/Cu(0). In molecular complexes, this feature highlights its tendency to decompose at the electrode surfaces with the loss of the free ligands and its nucleation as metallic copper clusters. However, the rigid covalent framework of PTI/Cu-high maintains the capability of the Cu cations to re-coordinate at the end of the cycle.

In summary, the crystalline poly(triazine imide) can coordinate to copper and then be electrophoretically deposited onto substrates, displaying cathodic current densities of >5 to 50 mA cm^{-2} for the reduction of protons and CO_2, the latter being favored for smaller particles. Its highly ordered structure has helped to reveal mechanistic insights into the CO_2R pathways relevant to Cu-containing complexes. Key discovered factors include the impact of multiple Cu coordination sites on the intermediate energies and CO_2 reduction products. These results thus provide fundamental, atomic-level understanding needed to optimize CO_2R, such as being explored in future research efforts aimed at monolayer-based PTI/Cu catalysts.

ASSOCIATED CONTENT

Supporting Information. Experimental and computational procedures, Rietveld refinements, elemental analysis, FT-IR, UV-Vis DRS, CO_2R product distributions, frontier molecular orbitals of intermediates, and reaction coordinate diagram. This material is available free of charge via the Internet at http://pubs.acs.org.

AUTHOR INFORMATION

Corresponding Author

* Email: paul_maggard@ncsu.edu

Author Contributions

The manuscript was written through contributions of all authors. All authors have given approval to the final version of the manuscript.

Funding Sources

U.S. Department of Energy, Office of Science, Office of Basic Energy Sciences under Award Number DE-SC0021173.

ACKNOWLEDGMENTS

This material is based upon work solely supported as part of the Center for Hybrid Approaches in Solar Energy to Liquid Fuels (CHASE), an Energy Innovation Hub funded by the U.S. Department of Energy, Office of Science, Office of Basic Energy Sciences under Award Number DE-SC0021173. SEM was carried out at the Analytical Instrumentation Facility (AIF) at North Carolina State University, and XPS was conducted at Duke University Shared Materials Instrumentation Facility (SMIF), supported by the state of North Carolina and the National Science Foundation (Award Number ECCS-2025064). The AIF and SMIF are members of the North Carolina Research Triangle Nanotechnology Network (RTNN), a site in the National Nanotechnology Coordinated Infrastructure (NNCI).

REFERENCES

1) Ju, W.; Bagger, A.; Hao, G.-P.; Varela, A.S.; Sinev, I.; Bon, V.; Cuenya, B.R.; Kaskel, S.; Rossmeisi, J.; Strasser, P. Understanding Activity and Selectivity of Metal-Nitrogen-Doped Carbon Catalysts for Electrochemical Reduction of CO_2. *Nat. Comm.* **2017**, *8*, 944.

2) Varela, A.S.; Ju, W.; Bagger, A.; Franco, P.; Rossmeisi, J.; Strasser, P. Electrochemical Reduction of CO_2 on Metal-Nitrogen-Doped Carbon Catalysts. *ACS Catal.* **2019**, *9*, 7270-7284.

3) Cometto, C.; Ugolotti, A.; Grazietti, E.; Moretto, a.; Bottaro, G.; Lidia Armelao, C.D.V.; Calvillo, L.; Granozzi, G. Copper Single-Atoms Embedded in 2D Graphitic Carbon Nitride for the CO_2 Reduction. *Npj 2D Mater. Appl.* **2021**, *63*, 1-11.

4) Ding, C.; Feng, C.; Mei, Y.; Liu, F.; Wang, H.; Dupuis, M.; Li, C. Carbon Nitride Embedded with Transition Metals for Selective Electrocatalytic CO_2 Reduction. *Appl. Catal. B: Env.* **2020**, *268*, 118391.

5) Yu, H.; Cohen, H.; Neumann, R. Photoelectrochemical Reduction of Carbon Dioxide with a Copper Graphitic Carbon Nitride Photocatahode. *Chem. Eur. J.* **2021**, *27*, 13513-13517.

6) Paul, S.; Kao, Y-L.; Ni, L.; Ehnert, R.; Herrmann-Geppert, I.; Krol, R.; Stark, R.W.; Jaegermann, W.; Kramm, U.I.; Bogdanoff, P. Influence of the Metal Center in M-N-C Catalysts on the CO_2 Reduction Reaction on Gas Diffusion Electrodes. *ACS Catal.* **2021**, *11*, 5850.

7) Lau, V.W.; Lotsch, B.V. A Tour-Guide Through Carbon Nitride-Land: Structure- and Dimensionality-Dependent Properties for Photo(Electro)Chemical Energy Conversion and Storage. *Adv. Energy Mater.* **2022**, *12*, 2101078.

8) Wirnhier, E.; Döblinger, M.; Gunzelmann, D.; Senker, J.; Lotsch, B.V.; Schnick, W. Poly(Triazine Imide) with Intercalation of Lithium and Chloride Ions $[(C_3N_3)_2(NH_2Li_{1-x})_3 \cdot LiCl]$: A Crystalline 2D Carbon Nitride Network. *Chem. Eur. J.* **2011**, *17*, 3213-3221.

9) Mesch, M.B.; Bärwinkel, K.; Krysiak, Y.; Martineau, C.; Taulelle, F.; Neder, R.B.; Kolb, U.; Senker, J. Solving the Hydrogen and Lithium Substructure of Poly(Triazine Imide)/LiCl Using NMR Crystallography. *Chem. Eur. J.* **2016**, *22*, 16878-16890.

10) Pauly, M.; Kroger, J.; Duppel, V.; Murphey, C.; Cahoon, J.; Lotsch, B.V.; Maggard, P.A. Unveiling the Complex Configurational Landscape of the Intralayer Cavities in a Crystalline Carbon Nitride. *Chem. Sci*, **2022**, *13*, 3187-3193.

11) Wang, J.; Hao, D.; Ye, J.; Umezawa, N. Determination of Crystal Structure of Graphitic Carbon Nitride: Ab Initio Evolutionary Search and Experimental Validation. *Chem. Mater.* **2017**, *29*, 2694–2707.

12) Suter, T.M.; Miller, T.S.; Cockcroft, J.K.; Aliev, A.E.; Wilding, M.C.; Sella, A.; Cora, F.; Howard, C.A.; McMillan, P.F. Formation of Ion-Free Crystalline Carbon Nitride and its Reversible Intercalation with Ionic Species and Molecular Water. *Chem. Sci.* **2019**, *10*, 2519.

13) Kim, K.; Wagner, P.; Wagner, K.; Mozer, A.J. Electrochemical CO_2 Reduction Catalyzed by Copper Molecular Complexes: The Influence of the Ligand Structure. *Energy Fuels* **2022**, *36*, 4653-4676.

14) Weng, Z.; Wu, Y.; Wang, M.; Jiang, J.; Yang, K.; Huo, S.; Wang, X.-F.; Ma, Q.; Brudvig, G.W.; Batista, V.S.; Liang, Y.; Feng, Z.; Wang, H. *Nat. Comm.* **2018**, *9*, 415

15) Besra, L.; Liu, M. A Review on Fundamentals and Applications of Electrophoretic Deposition (EPD). *Prog. Mat. Sci.* **2007**, *52*, 1-61.

16) Xu, J.; Shalom, M. Electrophoretic Deposition of Carbon Nitride Layers for Photoelectrochemical Applications. *ACS Appl. Mater. Interfaces* **2016**, *8*, 13058-13063.

17) Biesinger, M. C. Advanced Analysis of Copper X-Ray Photoelectron Spectra. *Surf. Interface Anal.* **2017**, *49*, 1325–1334.

18) Onida, G.; Reining, L.; Rubio, A. Electronic excitations: density-functional versus many-body Green's-function approaches. *Rev. Mod. Phys.* **2002**, *74*, 601-659

19) Perdew, J. P.; Ernzerhof, M.; Burke, K. Rationale for mixing exact exchange with density functional approximations. *J. Chem. Phys.* **1996,** *105*, 9982-9985

20) Carnimeo, I.; Baroni, S.; Giannozzi, P. Fast hybrid density-functional computations using plane-wave basis sets. *Electr. Struct.* **2019**, *1*, 015009.

21) Deslippe, J.; Samsonidze, G.; Strubbe, D. A.; Jain, M.; Cohen, M. L.; Louie, S. G., BerkeleyGW: A massively parallel computer package for the calculation of the quasiparticle and optical properties of materials and nanostructures. *Comp. Phys. Comm.* **2012,** *183*, 1269-1289.

22) Nitopi, S.; Bertheussen, E.; Scott, S.B.; Liu, X.; Engstfeld, A.K.; Horch, S.; Seger, B.; Stephens, I.E.L.; Chan, K.; Hahn, C.; Nørskov, J.K.; Jaramillo, T.F.; Chorkendoff, I. Progress and Perspectives of Electrochemical CO_2 Reduction on Copper in Aqueous Electrolyte. *Chem. Rev.* **2019**, *119*, 7610-7672.

SYNOPSIS. Soft electrophoretic deposition of crystallites of Cu-containing carbon nitride (inset) and their electrocatalytic activity for CO_2 reduction in aqueous solutions.